Heliyon 8 (2022) e12260

Contents lists available at ScienceDirect

Heliyon

journal homepage: www.cell.com/heliyon

Research article

Modelling of a linear ion trap operation in the second stability region

N.V. Konenkov [a], C.-F. Ding [b], A.N. Konenkov [a,*]

[a] Phys&Math Department, Ryazan State University, Svoboda str., 46, Ryazan, 390000, Russia
[b] School of Materials Science and Chemical Engineering, Institute of Mass Spectrometry, Ningbo University, Ningbo 315211, China

ARTICLE INFO

Keywords:
Linear ion trap
Dipolar excitation
The second stability region
Resolution
Excitation time
Excitation contour

ABSTRACT

Ion trajectory numerical simulation is used to find the linear ion trap excitation contour in the second stability region. The effects of initial conditions, the ejection Mathieu parameter, scan speed, dipole excitation voltage and gas damping are studied. Modeling shows that in the stability region center the resolution power is ≈ 200 000 (at full width half height of a peak, FWHM) at pressure 0.1 mTorr and 100 % excitation efficiency (not taking into account the space charge).

1. Introduction

The operation of the linear ion trap in the first stability region is described in detail in [1, 2]. The method of the resonance ion excitation by an auxiliary dipolar AC potential has been proposed by Fisher in 1959 [3]. The resonances take place on the ion secular motion frequencies $\omega_k = \frac{|2k+\beta|\Omega}{2}$, $k = 0, \pm1, \pm2, \ldots$, where β the characteristic exponent for the Mathieu parameter is a=0, Ω is the angle frequency of the RF drive potential. With increase of k the amplitudes of the ion secular oscillations in radial directions decrease and as a result the share of resonantly excited ions also drops. In practice, the fundamental frequency $\omega_0 = \frac{\beta\Omega}{2}$ is used [1]. For $a = 0$ values $\beta_x = \beta_y = \beta(q)$, where $q = \frac{4eV}{m\Omega^2 r_0^2}$, e and m are ion charge and mass, V is RF amplitude, r_0 is the field radius. Ions of a given mass number M are mass-selectively ejected from linear ion trap (LIT) if $= \frac{4eVN_A}{q_{ej}\Omega^2 r_0^2}$, where $q_{ej} = q\left(\frac{2\omega_0}{\Omega}\right)$ is called the ejection parameter [1], N_A is the Avogadro constant.

The linear quadrupole with dipole resonance excitation and mass selective with axial or radial ejection of the confined ions from ion trap are used in practice [4, 5, 6, 7]. The main advantages compared with the DC quadrupole are simplicity of using RF supply only, high resolution R = 6000, high scan speed 10^4 Th/s, small inertial process of the ion detecting, simple resonance circuit of the dipolar excitation of ions [8, 9, 10, 11].

Here we discuss RF-only mass-selective ejection of ions trapped in LIT operated in the second stability region [12]. A simple formula for the LIT resolution power R [13, 14, 15] is used

$$R = Cq_{ej}n\beta'\left(q_{ej}\right), \tag{1}$$

where C is a constant to be defined from experiment, q_{ej} is the ejection parameter, n is the excitation time expressed in RF cycles of the main trapping voltage, $\beta'(q_{ej})$ is derivative of the function $\beta(q)$ at the point $q = q_{ej}$. The value $\beta'(q_{ej})$ determines the dispersion between the excitation frequency and the ion mass. It can be expected that the resolution of the LIT is substantially higher in the second stability region than in the first stability region because $q_{ej}(\mathrm{II}) \cong 7.55 \gg q_{ej}(\mathrm{I}) \cong 0.75$. This fact can be used as a starting point for the study of the linear trap operation in the second stability region.

2. Stability region II

Region II is a triangle on the (a,q) plane with $7.514 < q < 7.580$ [11]. Parameter β takes values between 1 and 2 (Figure 1). The iso-β_x and iso-β_y lines are shown with dotted lines. Dipole resonance excitation of ion oscillations can be realized at any point (a,q) of the stability region by using an additional DC potential $\pm U$ at the electrodes and an additional RF voltage at the opposite electrodes at the frequency $\beta_x\Omega/2$ or $\beta_y\Omega/2$. However, a simpler technical solution of resonant excitation is attainable when there is no DC potential and $a = 0$.

The graph of the function $\beta'(q)$ for the case $a = 0$ is given on Figure 2. The derivative $\beta'(q)$ tends to infinity when q approaches the boundary values $q = 7.514$ and $q = 7.580$. At the center $(q_{ej} = 7.547)$

* Corresponding author.
E-mail address: n.konenkov@365.rsu.edu.ru (A.N. Konenkov).

https://doi.org/10.1016/j.heliyon.2022.e12260
Received 23 July 2022; Received in revised form 29 October 2022; Accepted 2 December 2022

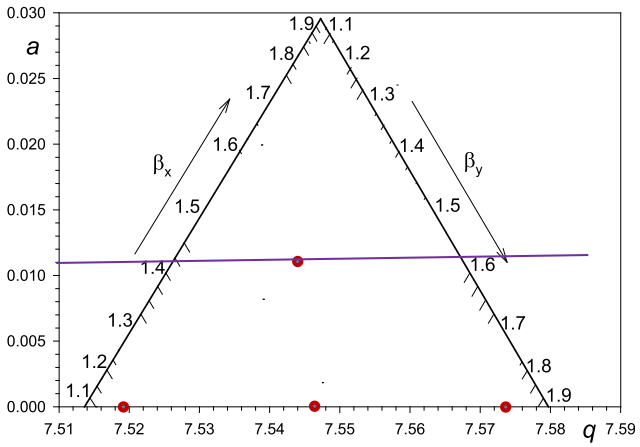

Figure 1. The second stability region on the (a, q) plane. The dashed lines are iso-β lines. Below we use the operating points with the following a, q excitation parameters: $a = 0, q = 7.752$, $\beta = \beta_x = \beta_y = 1.2; a = 0, q = 7.547, \beta = \beta_x = \beta_y = 1.5; a = 0, q = 7.5735, \beta = \beta_x = \beta_y = 1.8$; $a = 0.011, q = 0.7547, \beta_x = 1.6, \beta_y = 1.3575$.

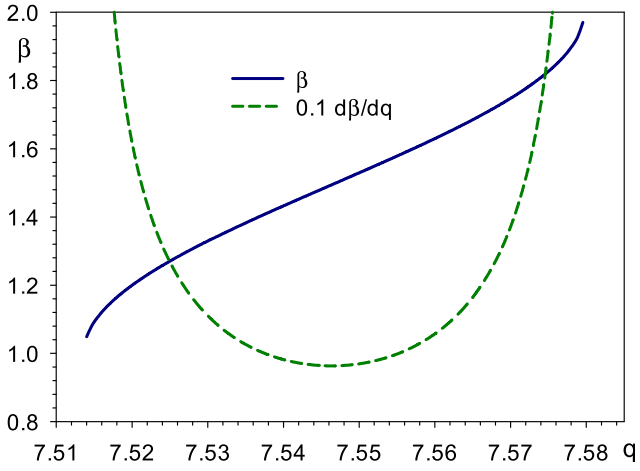

Figure 2. Function $\beta(q)$ and its derivative $\beta'(q)$ in the second stability region.

of the stability region $\beta'(q) \cong 9.65$. Thus according to Eq. (1) the resolution $R = C9.65 q_{ej} n$.

2.1. Ion motion equations and excitation contour

The motion equations in the radial plane of a linear RF quadrupole with auxiliary dipole excitation are [2, 13]:

$$x'' + \{a - 2q\cos[2(\xi - \xi_0)]\} + 2q_x \cos[2\nu(\xi - \xi_0)] = 0, \quad (2)$$

$$y'' - \{a - 2q\cos[2(\xi - \xi_0)]\}y = 0, \quad (3)$$

where

$$q = \frac{4eV}{\left(\frac{m}{z}\right)\Omega^2 r_0^2}, \quad (4)$$

$$q_x = \frac{A_1 V_{ex}}{2V} q. \quad (5)$$

In Eqs. (2) and (3) q is the Mathieu parameter, $\xi = \Omega t/2$ is the dimensionless time, x and y are transverse Cartesian coordinates, ξ_0 is the initial RF phase, e is the magnitude of the electronic charge, m/z is the ion mass-to-charge ratio, V and Ω are, respectively, the amplitude zero to peak, pole to ground, and the angular frequency of the trapping RF field. The field radius of the quadrupole r_0 is the distance from the quadrupole central axis to an electrode. Excitation parameter q_x depends on amplitude V_{ex} of the dipole potential $V_{ex} \cos \omega t$ as given in Eq. (5). Normalized dipolar amplitude of the first spatial harmonic generated by round rods is $A_1 = 0.798$. Dimensionless excitation frequency is $\nu = \frac{\omega}{\Omega} = \beta/2$.

We take the excitation contour $S(q)$ as a general characteristic of the ejection process, see [13] for the first stability region. It is defined as $S(q) = N_{ex}/N$, where N_{ex} is the number of ion trajectories for which $|x(\xi)| \geq 1, \xi \leq n\pi$ and N is the total number of ions trajectories. The most interest has a peak which reaches the maximum resolution for $S = 100\%$. It touches the level $S = 100\%$ at one point only and depends on the excitation time n and the excitation relative amplitude q_{ex}. Initial transverse ion positions and velocities are normally distributed and initial RF phases are uniformly distributed on the interval $(0, \pi)$ [13]. The dimensionless velocity mean square deviation is [13]

$$\sigma_v = \sqrt{(k_B T_i N_A/M)} \Big/ (\pi r_0 f),$$

where k_B is the Boltzmann constant, N_A is the Avogadro constant, T_i is ion temperature, M is the mass number, $f = \Omega/2\pi$ is the cycle frequency. The initial x_0 and y_0 coordinates are distributed normally with variances $\sigma_x^2 = \sigma_y^2$ expressed in units of r_0. For ion mass $M = 609$ Th with ion temperature $T_i = 300\ K$, $r_0 = 3$ mm, $f = 0.5$ MHz the mean square deviation $\sigma_v = 0.0096$.

As an example, we will estimate the parameters of an ion trap for resonant detection of ions with mass M = 609 Th. Take the RF generator frequency $f = 2\pi/\Omega = 500$ KHz, $r_0 = 3$ mm, $q_{ej} = 7.547$. Then the amplitude of the RF voltage is $V = 1060$ V. At $q_{ej} = 7.547$ the dipole frequency is $f_{ex} = \frac{\beta f}{2} = 375$ KHz for the parameter $\beta = 1.5$. The parameters are technically feasible. The dipole voltage V_x is determined by the value of q_x, which is found from simulation.

2.2. Excitation contours

The mass peaks are presented on Figure 3 for given values of the excitation time n expressed in RF cycles. The contours have tails which are not observed in the first stability region [13]. From Figure 3 it follows that the separation time n and the excitation parameter q_{ex} are related as $nq_{ex} \cong 0.0306$. The characteristic exponent $\beta = 3/2$ coresponds to the ejection parameter $q_{ej} = 7.54696$. The required amplitude V_x of the dipole potential for the given conditions, see (4) and (5), is given by

$$V_x = \frac{2Vq_{ex}}{A_1 q_{ej}} \frac{1}{n} \cong \frac{0.0306*2*1060}{0.798*7.547} \frac{1}{n} \cong \frac{11}{n}\ (Volt).$$

These data (рис. 3) are well approximated by a linear function (Figure 4). Using formula (1) we evaluate the adjustable constant C:

$$10 q_{ej} \beta'(q) nC = 30n$$

and $R_{0.5} \cong 2.5 q_{ej} \beta'(q)\, n$. For the first stability region $q_{ej} = 0.85$ and the resolution $R_{0.5} \cong 2\, q_{ej} \beta'(q)\, n = 1.63\, n$ [13]. The resolution for the second stability region is $30/1.63 \cong 18$ times higher compared with the first stability region. For example, excitation time $n = 100$ corresponds to $5*10^3$ Th/s ($f = 0.5*10^6$ Hz) and resolution $R_{0.5} = 2540$ (Figure 3). The resolution is equal to 150 000 for small scan speed 100 Th/s (n = 5000).

Note that the excitation contours in Figures 3 and 5 correspond to 100% excitation level when all ions are unstable. Since the top of the contour is flat (Figure 5a), the 100% excitation level was determined approximately. The resolution $R_{0.5}$ (FWHM) is determined for these conditions. Figure 5a shows the transmission contours for $\beta = 1.2$ at the point $q = 2.520$ (Figure 1) when the dispersion $d\beta/dq$ increases (Figure 2). The resolution increases to $R_{0.5} = 18\,300$ compared to the

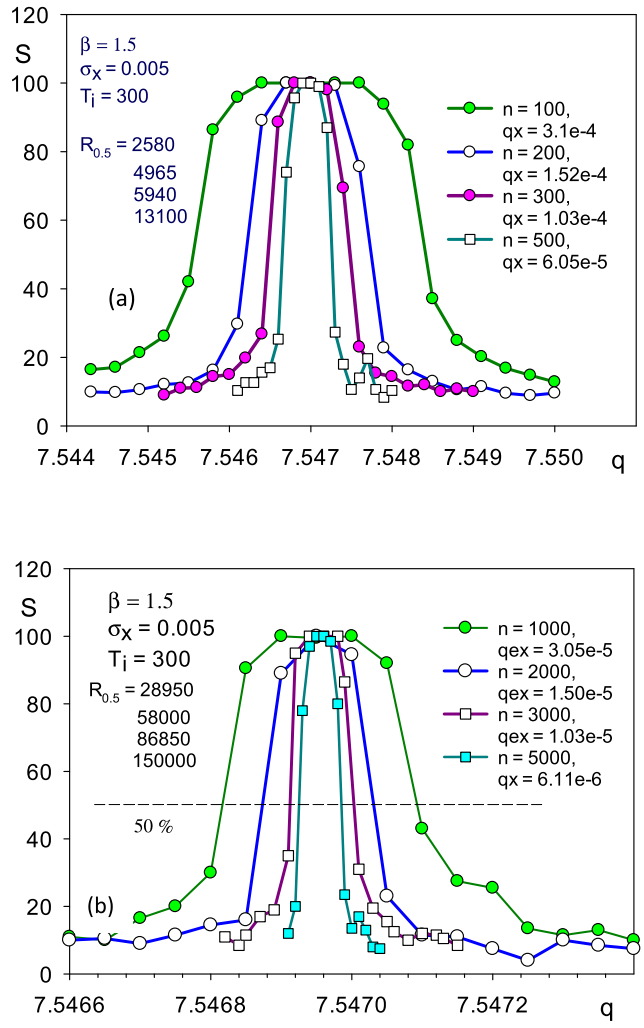

Figure 3. Contours (mass peaks) for excitation time (a) $n = 100, 200, 300, 500$ and$(b)1000, 2000, 3000$ and 5000 RF cycles; n is the excitation time; q_{ex} is the dimensionless dipole amplitude; $\nu = \frac{3}{4}$; $nq_{ex} \cong 0.0306$; $R_{0.5}$ is the resolution (FWHM). 1000 ion trajectories per point.

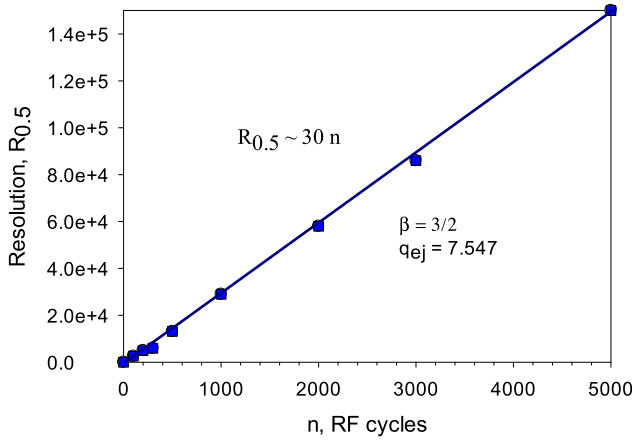

Figure 4. Linear dependence of the resolution $R_{0.5}$ on the excitation time n for $= 3/2$, $q_{ej} = 7.5469$.

case $\beta = 1.5$ (Figure 3a, $n = 500$) when $R_{0.5} = 13\,100$ according to Figure 2. However, on the small q side, the noise pedestal increases sharply and the closer the operating point to the boundary of the region $\beta = 1.0$, the greater the pedestal's height.

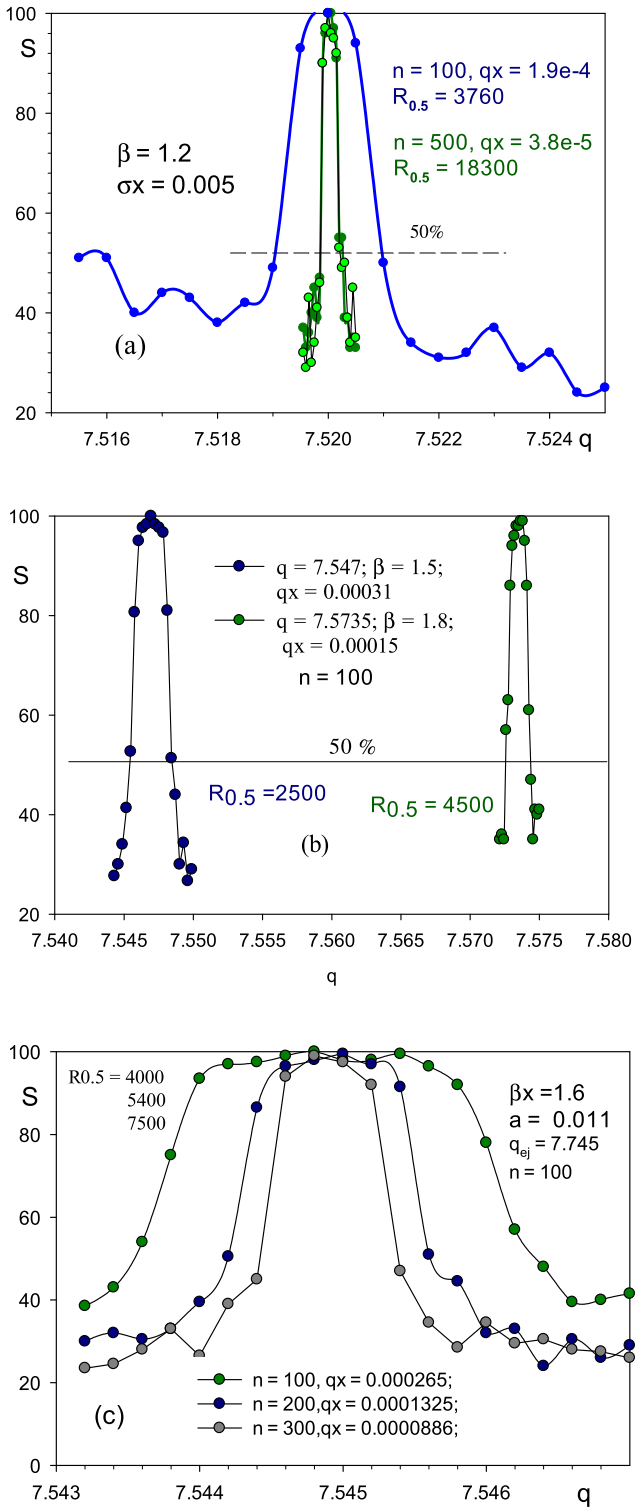

Figure 5. Excitation contours under the following conditions and parameter values: (a) $\beta = 1.2$; (b) $\beta = 1.8$ and (c) $\beta_x = 1.6$ (a = 0.011, $q = 7.745$).

Figure 5b gives a comparison of the excitation contours in the working points $\beta = 1.5$ and $\beta = 1.8$ (Figure 1) for the case $n = 100$, when the scanning speed is very high: $f/n = 5000$ Th/s. When the parameter β approaches the right stability boundary (Figure 1, value $\beta = 2$) the dispersion $d\beta/dq$ increases (Figure 2), the resolution also increases from 2500 (for $\beta = 1.5$) to 4500 with the amplitude q_x halved.

For the case of the operating point $a = 0.011, q = 7.745$ ($\beta_x = 1.6$) inside the stability region (Figure 1), the transmission contours for

$n = 100$, 200 and 300 are shown in Figure 5c. The resolution is of the same order as for the case $\beta_x = 1.2$ and $\beta_x = 1.8$ (Figure 5a and b).

2.3. Influence of the buffer gas pressure on the excitation contour

Consider the motion of $M = 609$ Th ions under the conditions stated above. To calculate the trajectories of ions in the buffer gas, we use the equations of motion presented in [13, 16]. Figure 6 shows the excitation contours for pressures $p = 0, 5, 7$ and 9 mTorr at fixed values of dimensionless dipole excitation amplitude $q_x = 3.1 \times 10^{-4}$ and the excitation time $n = 100$. In Figure 6a the dispersion value $\sigma_x = 0.01$ and in Figure 6b $\sigma_x = 0.005$. These values characterize the radial dimensions of the ion cloud before the dipole resonance effect on the selected ions. It follows from the data in Figure 5 that the presence of a buffer gas leads to an increase in the resolving power of $R'_{0.5} = \frac{q_{ej}}{\Delta q}$, when the peak height is counted from the baseline. The baseline passes through the noise pedestal (Figure 5a for curve 9 mTorr). With this determination of resolution, the value of $R'_{0.5}$ increases from 2800 to 8300 with a high scanning rate of 5000 Th/c (Figure 5a). The noise pedestal also decreases with increasing pressure. Increasing the near-axis ion concentration ($\sigma_x = 0.005$, Figure 5b) decreases the noise pedestal and increases the resolving power in the presence of pressure. The presence of gas pressure in the ion trap gives approximately the same 95% excitation intensity and approximately the same resolving power $R_{0.5} \cong 4400$ at two values of the near-axis localization of the ion cloud $\sigma_x = 0.01$ and $\sigma_x = 0.005$.

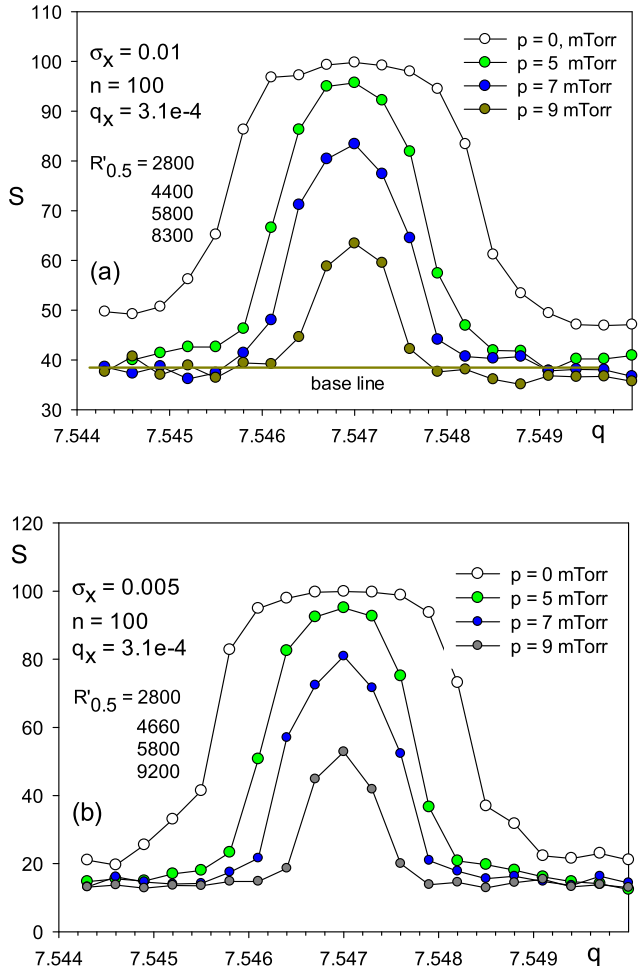

Figure 6. The influence of the buffer gas pressure on the excitation circuit: radial distribution of argon atoms, characterized by the standard deviation (a) $\sigma_x = 0.01$ and (b) $\sigma_x = 0.005$.

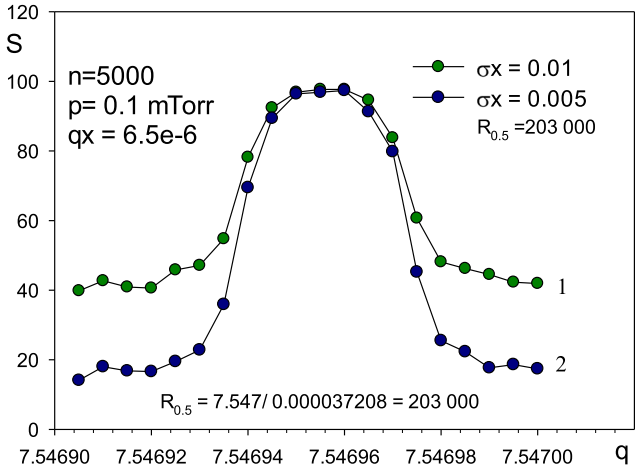

Figure 7. Excitation contour for slow scan speed 100 Th/s ($n = 5000$) and small damping gas pressure $p = 0.1$ mTorr. Dipole voltage amplitude $V_x = 2.34$ mV ($q_x = 6.05 \times 10^{-6}$). 1) $\sigma_x = 0.01$; 2) $\sigma_x = 0.005$.

An excitation contour with high resolution $R_{0.5} = 203,000$ and 100% (S ≅ 100) excitation efficiency is illustrated in Figure 7 (curve 2). The presence of a small buffer gas pressure $p = 0.1$ mTorr results in a 25% increase in resolution compared to the case when no gas damping. In Figure 7, curve 2 is obtained for the near-axis distribution of ions with $\sigma_x = 0.005$. The resonant long-term ($n = 5000$) interaction of an ion ensemble with a more rarefied buffer gas requires an increase in the dipole voltage amplitude from 2.20 mV to 2.34 mV. As σ_x is doubled (contour 1), the intensity of the noise pedestal also doubles, which is characteristic of the stability region I too [13]. The dipole voltage increases approximately linearly with increasing pressure and constant scan speed.

3. Discussion and conclusion

We consider the excitation contour of a linear ion trap operated in the second stability region. It is shown that in the absence collisional damping the mass peak width depends mainly on the excitation time, which is controlled by the scan speed. The resolution $R_{0.5}$ has a linear dependence $R_{0.5} \sim 30\,n$ for $q_{ej} = 7.547$. The separation time n and excitation parameter q_{ex} are related as $nq_{ex} \cong 0.0306$.

The operation of the LIT at the working points near the boundaries of the stability region leads to the appearance of powerful noise pedestals on the excitation contour, inside the region - the pedestals remain at the level of 20% of the contour height. Buffer gas pressure in the LIT results in lowering the baseline and increasing the resolving power. So at a high scanning speed of 5000 Th/s, dipole voltage amplitude of 11 V and argon pressure of 9 mTorr, the resolving power $R_{0.5} \cong 9200$ for ions with $M = 609$ Th and LIT parameters $f = 0.5$ MHz, $r_0 = 3$ mm and $V = 1060$ V. For the case of a slow scanning speed of 100 Th/s with a buffer gas pressure of 0.1 mTorr the resolution $R_{0.5} = 203{,}000$ at amplitude $V_x = 2.34$ mV. So to achieve in the first region stability, for example $R_{0.5} = 30,000$ requires high dipole voltage stability $\Delta q_x/q_x \sim 10^{-3}$ (see Figure 15 [13] and Figure 3 [8]). The nature of the influence of pressure, scanning speed, and dipole voltage amplitude on the excitation contour is the same as for the case of the first stability region.

Declarations

Author contribution statement

Nikolai Konenkov: Conceived and designed the experiments; Wrote the paper.

Chuan-Fan Ding: Contributed reagents, materials, analysis tools or data; Analyzed and interpreted the data.

Andrei Konenkov: Performed the experiments.

Funding statement

This research did not receive any specific grant from funding agencies in the public, commercial, or not-for-profit sectors.

Data availability statement

No data was used for the research described in the article.

Declaration of interest's statement

The authors declare no competing interests.

Additional information

No additional information is available for this paper.

References

[1] R.E. March, Quadrupole ion traps, Mass Spectrom. Rev. 28 (2009) 961–989.
[2] P.M. Remes, J.E.P. Syka, V.V. Kovtoun, J.C. Schwartz, Insight into the resonance ejection process during mass analysis through simulations for improved linear quadrupole ion trap mass spectrometer performance, Int. J. Mass Spectrom. 370 (2014) 44–57.
[3] E. Fischer. Die dreidimensionale stabilisierung von ladungsträgern in einem vierpolfeld. Z. Phys., 156 (959), pp. 1-30.
[4] J.W. Hager, Performance optimization and fringing field modifications of a 24-mm long rf-only quadrupole mass spectrometer, Rapid Commun. Mass Spectrom. 13 (12) (1999) 1205–1208.
[5] F.A. Londry, J.W. Hager, Mass selective axial ion ejection from a linear quadrupole ion trap, J. Am. Soc. Mass Spectrom. 14 (2003) 1130–1147.
[6] J.C. Schwartz, M.W. Senko, J.E.P. Syka, A two dimensional quadrupole ion trap mass spectrometer, J. Am. Soc. Mass Spectrom. 13 (2002) 659–669.
[7] D.J. Douglas, A.J. Frank, D. Mao, Linear ion traps in mass spectrometry, Mass Spectrom. Rev. 24 (1) (2005) 1–29.
[8] J.C. Schwartz, J.E.P. Syka, I. Jardine, High resolution on a quadrupole ion trap mass spectrometer, J. Am. Soc. Mass Spectrom. 2 (1991) 198–204.
[9] D.E. Goeringer, W.B. Whitten, J.M. Ramsey, S.A. McLuckey, G.L. Glish, Theory of high-resolution mass spectrometry achieved via resonance ejection in the quadrupole ion trap, Anal. Chem. 64 (1992) 1434–1439.
[10] S.M. Williams, K.W.M. Siu, F.A. Londry, V.I. Baranov, Resonant excitation by linear ion trap simulations, J. Am. Soc. Mass Spectrom. 18 (2007) 578–587.
[11] R.E. March, R.J. Hughes, Quadrupole Storage Mass Spectrometry, John Wiley & Sons, New York, 1989, p. 44.
[12] C.C. Grimm, R. Clawson, R.T. Short, Use of region II of the a/q stability diagram for fast scanning of a linear quadrupole mass spectrometer, J. Am. Soc. Mass Spectrom. 8 (1997) 539–544.
[13] D.J. Douglas, N.V. Konenkov, Mass selectivity of dipolar resonant excitation in a linear quadrupole ion trap, Rapid Commun. Mass Spectrom. 28 (2014), 430–429.
[14] B.A. Collings, W.R. Stott, F.A. Londry, Resonant excitation in a low pressure linear ion trap, J. Am. Soc. Mass Spectrom. 14 (2003) 622–634.
[15] N.S. Arnold, G. Hars, H.L.C. Meuzelaar, Extended theoretical considerations for mass resolution in the resonance ejection mode of quadrupole ion trap mass spectrometry, J. Am. Soc. Mass Spectrom. 5 (1994) 676–688.
[16] I.V. Kurnin, M.I. Yavor, Peculiarities of ion beam transport in gas-filled quadrupoles at intermediate pressure values, Rus. J. Tech. Phys. 79 (2009) 112–119.